



Mapping mangrove disturbance state using decision tree classification based on Sentinel-2 surface reflectance spectral indices, elevation, and salinity data in the Parc Marin des Mangroves (Moanda, Democratic Republic of Congo)

Raymond Lumbuenamo Sinsi^{1,2*}, Elie Nsimba Ngembo^{1,2*}, Eric Lutete Landu¹, Arielle Mabaya¹, Bonaventure Lele Nyami¹, Cedric Kompani Daba¹, Arsène Kayengi Baziot¹, Dan Lusolamo Nguizani¹, Giresse Bifubiambote Salambiaku³, Louis Ngeli Mpayi⁴, Hippolyte Ditona Tsumbu², Roger Ntoto M'Vubu³

⁽¹⁾University of Kinshasa. Faculty of Agricultural and Environmental Sciences. Department of Natural Resources Management. BP 117 Kinshasa XI (DRC). E-mail : raymond.lumbuenamo@unikin.ac.cd ; elie.ngembo@unikin.ac.cd

⁽²⁾Regional School for Integrated Planning and Management of Tropical Forests and Territories. BP 15373-Kinshasa (DRC)

⁽³⁾University of Kinshasa. Faculty of Agricultural and Environmental Sciences. Department of Agricultural Economy. BP 117 Kinshasa XI (DRC)

⁽⁴⁾Congolese Institute for Nature Conservation, Parc Marin des Mangroves. BP 16576 Kin 1 (DRC)

Reçu le 21 mai 2025, accepté le 21 mai 2025, publié en ligne le 28 juin 2025

DOI : <https://dx.doi.org/10.4314/rafea.v8i2.15>

ABSTRACT

Description of the subject. Despite increased human pressures, few studies have characterized disturbance states of mangroves using local ecological conditions, such as those of the Parc Marin des Mangroves (PMM) in the Congo Basin.

Objectives. Assess the state of the mangrove stands disturbance in the PMM by: (a) analyzing elevation, salinity, and spectral indices variability, (b) mapping mangrove disturbance, and (c) estimating the area of each disturbance class.

Methods. Sentinel-2 surface reflectance data from March 2024 to March 2025 were used to compute three spectral indices: NDVI, NDMI, and CMRI. Elevation data were derived from the Shuttle Radar Topography Mission, and a spatial salinity model was interpolated from field water stream electrical conductivity measurements. The Global Mangrove Watch 2020 data defined the extent of mangroves. A decision tree classifier used thresholds for each variable: undisturbed mangroves had NDVI > 0.55, CMRI > 0.5, and NDMI > 0.1, while disturbed mangroves had NDVI between 0.3 and 0.55, CMRI > 0.3, and NDMI > 0.1. Non-mangrove areas included pixels below these thresholds. Mangroves were mapped between 0-46m of elevation with conductivity values higher than 30 $\mu\text{S}/\text{cm}$, including a mask of artefact values predicted within the mangrove area.

Results. Mangroves spanned 242.4 km², with 76.89 km² (10.53%) disturbed and 165.51 km² (22.68%) undisturbed. Non-mangrove areas totaled 487.24 km² (66.77%). After adjusted pixels area-bias correction, mangrove coverage was 242.46 \pm 11.98 km², with an overall accuracy of 96.90 %.

Conclusion. Local field inventories are essential to refine mangrove mapping and capture ecological nuances missed by global models.

Keywords: Decision Trees, mangrove mapping, spectral indices, Parc Marin des Mangroves/DRC

RESUME

Cartographie de l'état de perturbation des mangroves à l'aide d'une classification par arbre de décision basée sur les indices spectraux calculés à partir des images de réflectance de surface Sentinel-2, l'élévation et les données de salinité dans le Parc Marin des Mangroves (Moanda, République Démocratique du Congo)

Description du sujet. Malgré la pression humaine croissante, peu d'études ont caractérisé l'état de perturbation des mangroves considérant les conditions écologiques locales, telles dans le Parc Marin des Mangroves (PMM) dans le bassin du Congo.

Objectifs. Evaluer l'état de perturbation des peuplements de mangroves dans le PMM en : (a) analysant la variabilité de l'élévation, de la salinité et des indices spectraux, (b) cartographiant les perturbations des mangroves, et (c) estimant la superficie de chaque classe de perturbation.

Méthodes. Les données de réflectance de surface Sentinel-2 de mars 2024 à mars 2025 ont été utilisées pour calculer trois indices spectraux : NDVI, NDMI et CMRI. L'élévation a été obtenue via les données Shuttle Radar Topography Mission et un modèle spatial de salinité a été produit à partir des mesures de conductivité électrique de l'eau. Le masque de Global Mangrove Watch 2020 a délimité l'étendue des mangroves. Un arbre de décision a classifié les mangroves : non perturbées (NDVI > 0,55, CMRI > 0,5, NDMI > 0,1), perturbées (NDVI 0,3-0,55, CMRI > 0,3, NDMI > 0,1) et non-mangroves (en dessous de ces seuils). L'élévation étant fixée entre 0 et 46m pour les zones à mangroves avec une conductivité estimée supérieure à 30 $\mu\text{S}/\text{cm}$, y compris le masque des valeurs aberrantes prédites dans les zones à mangroves.

Résultats. Les mangroves couvraient 242,4 km², dont 76,89 km² (10,53 %) perturbées et 165,51 km² (22,68 %) non perturbées. Les zones non-mangroves totalisaient 487,24 km² (66,77 %). La couverture totale des mangroves était de $242,46 \pm 11,98$ km², avec une précision globale de 96,90 %.

Conclusion. Les inventaires de terrain sont essentiels pour affiner la cartographie des mangroves et capturer les nuances écologiques que les modèles globaux peuvent manquer.

Mots-clés : Arbres de décision, cartographie des mangroves, indices spectraux, Parc Marin des Mangroves/RDC

1. INTRODUCTION

Mangrove ecosystems are under increasing pressure due to anthropogenic and climate change effects, resulting in alarming deforestation and ecosystem degradation. Approximately 8,600 km² of the world's mangroves were lost between 1990 and 2020, with a notable acceleration in the South and Southeast Asian regions, which account for 54% of total losses (Bhowmik *et al.*, 2022).

Mangroves occur in the Congo Basin region in the Democratic Republic of Congo (DRC), where the Parc Marin des mangroves (PMM) was created to preserve the characteristic ecosystems of the Congo River estuary. Several studies report increasing pressures on this ecosystem (Muyaya *et al.*, 2017; Mbiya *et al.*, 2024). The PMM remains understudied, with limited data on its ecological functioning and socio-environmental context. Human activities, such as charcoal production, contribute to the degradation of this ecosystem. Characterizing the disturbance of mangrove stands is essential in the PMM.

In addition, mangroves are known for their ability to adapt to salinity, tidal variation, and other hydrodynamic conditions of the coastal landscape, which justifies the crucial role of water properties and hydrodynamic data in studying mangroves (Faye *et al.*, 2007; Risanti *et al.*, 2020; Allais *et al.*, 2024; Greenfield, 2024). Remote sensing approaches with high spatial and temporal resolution data are crucial for research and sustainable mangrove management under anthropogenic pressures and the effects of climate change (Baloloy *et al.*, 2020; Tran *et al.*, 2022; Sunkur *et al.*, 2024; Tran *et al.*, 2024).

Various spectral indices from satellite images may characterize the state of vegetation and its physiological functioning (Tran *et al.*, 2022). In addition to generic vegetation indices such as the

Normalized Difference Vegetation Index (NDVI) or the Soil-Adjusted Vegetation Index (SAVI), mangrove-specific indices have now been developed. These include the Mangrove Vegetation Index (MVI) (Baloloy *et al.*, 2020) and the Combined Mangrove Recognition Index (CMRI) (Gupta *et al.*, 2018).

Several studies have demonstrated differences in accuracy when mapping mangrove stands using generic indices or specific mangrove indices (Gupta *et al.*, 2018; Baloloy *et al.*, 2020; Tran *et al.*, 2024). However, this may be challenging in a complex landscape with mangrove and non-mangrove forest stands. Therefore, combining these indices for mapping mangroves may highlight statistical correlation issues. In this case, the decision trees (Breiman *et al.*, 1984) may help to overcome this by defining the threshold of each index value for each land cover class. They are better suited to handle highly correlated features (Kodikara and Woldai, 2017), such as spectral bands or indices, than many other models (Kavhu *et al.*, 2021). Decision trees handle correlated variables by (1) selective splitting, where only one variable is selected per split ; (2) non-linear thresholding, no assumption of linear or monotonic relationships; (3) no assumptions about independence (Breiman *et al.*, 1984; Cutler *et al.*, 2007; Hastie *et al.*, 2009).

This study employs the decision tree classification approach to map the state of mangrove stand disturbance. It aims to enhance the understanding of mangrove disturbance in the PMM using reflectance spectral indices, a salinity spatial model, and elevation data across global mangrove ecological conditions from the 2020 Global Mangrove Watch (GMW) layer (Bunting *et al.*, 2022). Three objectives are targeted and aim to (1) assess the terrain elevation, salinity, and spectral indices variability in the PMM, (2) map the state of

the mangrove disturbance, and (3) estimate the area of each mangrove's disturbance class.

This study will address two research questions: (1) What are the spatial variations of spectral indices, elevation, and salinity patterns of mangrove areas in the PMM? And (2) What is the state of disturbance of the mangrove forest in the PMM? The result of this research will guide restoration efforts in the PMM by highlighting the areas of disturbed mangrove.

2. MATERIAL AND METHODS

2.1. Study area

The PMM is located on the western side of the Democratic Republic of Congo (Figure 1), between 5.9182° and 6.06174° of southern latitude and

between 12.3481° and 12.6052° of eastern longitude, in the coastal landscape, with a mean annual temperature of 25.7 °C and 430.8-772 mm of rainfall. It hosts the mouth of the Congo River at the Atlantic Ocean. Few studies have been conducted on mangrove flora in the PMM. It is reported that *Rhizophora racemoza*, *Rhizophora mangle*, and *Avicennia germinans* are the most characteristic species. These mangrove-specific, forest trees, herbaceous, and other species make the PMM a complex vegetation ecosystem. Manatees, marine turtles, crocodiles, monkeys, and hippopotamuses are the most emblematic animals of the PMM. The landscape, precisely in the village of Nsiamfumu, is linked to the history of enslavement, where people were trafficked.

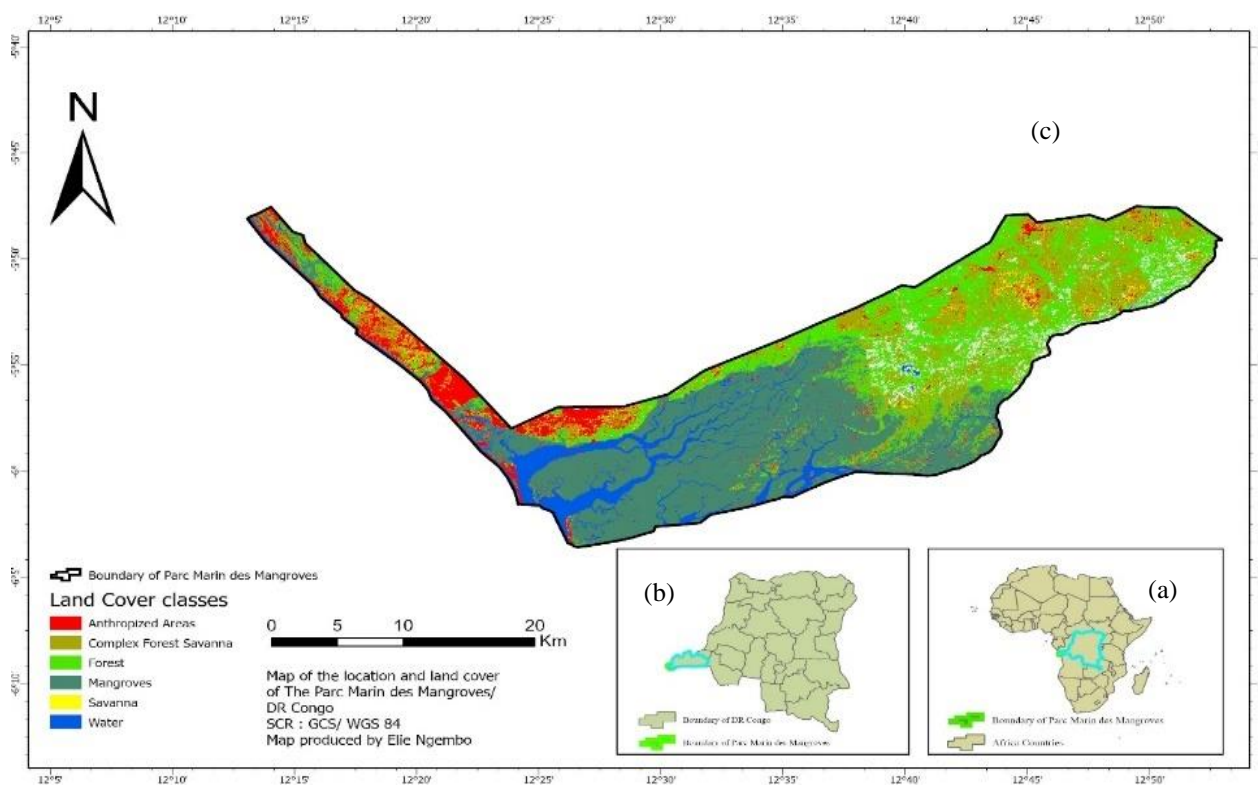


Figure 1. Location of the PMM in Africa (a), in the Democratic Republic of Congo and Kongo-Central province (b), land cover classes (c)

2.2. Data processing and mapping of mangrove disturbance state

We utilized Sentinel-2 surface reflectance data, comprising 10 m spatial resolution bands from the Google Earth Engine (GEE) (Gorelick *et al.*, 2017; Velastegui-Montoya *et al.*, 2023), acquired between March 2024 and 2025. From the Sentinel-2 data, we computed three spectral indices: NDVI (Normalized Difference Vegetation Index), NDMI (Normalized Difference Moisture Index), and CMRI (Combined Mangrove Recognition Index) using the median value of the selected period for each band concerned. NDVI is a vegetation health

monitoring index (Rouse *et al.*, 1973), CMRI is a specific mangrove monitoring index, and NDMI highlights the moisture content of vegetation.

The CMRI aims to improve the accuracy of mangrove mapping by leveraging the strengths of NDVI on the NDWI (Normalized Difference Water Index). NDVI and NDWI have a strong inverse correlation ($r = -0.988$) (Gupta *et al.*, 2018), which led to the development of a simple algorithm that subtracts NDWI values from NDVI at the pixel level to enhance the distinction between mangrove and non-mangrove areas (Gupta *et al.*, 2018). The NDVI is computed using the expression: $NDVI =$

$(\text{NIR} - \text{Red}) / (\text{NIR} + \text{Red})$, where NIR is the Near-Infrared Band (e.g., Sentinel-2 Band 8) and Red refers to the Red Band (e.g., Sentinel-2 Band 4).

The NDWI is computed using $\text{NDWI} = (\text{Green} - \text{NIR}) / (\text{Green} + \text{NIR})$, with Green = Green Band (e.g., Sentinel-2 Band 3). The CMRI is calculated as follows: $\text{CMRI} = \text{NDVI} - \text{NDWI}$. The NDMI is calculated as $\text{NDMI} = (\text{NIR} - \text{SWIR}) / (\text{NIR} + \text{SWIR})$, where SWIR is the shortwave infrared band (e.g., Sentinel-2 band 11).

A salinity model was produced by interpolating the water electrical conductivity (EC) field data, serving as a proxy, collected during high-tide times. EC data were collected from freshwater to saltwater transects through a field stream water monitoring survey. It also covered some temporarily flooded land outside of the stream. Water EC measurement points along the stream were taken at an average interval of three minutes between consecutive measurements. Handling the boat driver's speed in strong waves and a high-tide hydrodynamic context was sometimes challenging. Sixty-four water EC measurements were collected during the field survey from the freshwater (boma and surroundings) and Atlantic Ocean water (Tshende village) using a water multiprobe Hanna Instrument HI98192 between September and October 2023.

The EC spatial model was produced using the Kernel Interpolation with Barriers (KIB) algorithm, which was selected as the model with the lowest Root Mean Square Error (RMSE). We assessed four interpolators using the ArcGIS 10.8 software: Inverse Distance Weighted, Kriging, Local Polynomial Interpolator, and KIB. To determine the quality of interpolation results, we have performed an interpolation cross-validation using the geostatistical toolbox, utilities toolset, and cross-validation tool. The best model in this case was KIB, which had the lowest RMSE value. The KIB was applied to a polynomial five kernel function. The ridge parameter, an optional setting used for numerical stabilization, was set to the default parameter of fifty. All other interpolation parameters were optional and defaulted to the values presented by the software.

Some negative values were observed in the interpolation results. After analyzing these values, it was noted that they are observed in the Global Mangroves Watch (GMW) extent in the PMM, specifically in the transition between oligohaline (lower salinity content) and freshwater. To prevent losing these pixels, we masked these values by applying the $\text{EC} < 0$ expression, which is accounted for in the classification. Applying a mask to handle artifacts interpolated values was suggested by Zhang *et al.* (2015), Martínez-Fonseca *et al.* (2024), and Martínez *et al.* (2024). Merow *et al.* (2022) have also suggested mask application to manage

environmental outliers in species distribution models.

To classify water salinity, EC values ($\mu\text{S}/\text{cm}$) were converted to total dissolved solids (TDS) in parts per million (ppm) using an empirical relationship specific to sodium chloride (NaCl) solutions: $100 \mu\text{S}/\text{cm} = 64 \text{ ppm TDS}$ (Apha *et al.*, 2017). TDS values were then converted to salinity in parts per thousand (ppt) by dividing by 1.000, to align with the Venice System for the Classification of Marine Waters according to salinity (UNESCO, 1958). This system defines salinity classes as follows: (a) oligohaline: 0.5–5 ppt, (b) mesohaline: 5–18 ppt, (c) polyhaline: 18–30 ppt, (d) euhaline (typical seawater): 30–40 ppt and finally (d) hyperhaline: > 40 ppt. This approach will enable us to identify the locations of mangrove areas along the EC-derived salinity classes.

The SRTM USGS (Shuttle Radar Terrain Model from the United States Geological Survey) digital elevation data, available in GEE with a spatial resolution of 30 m, was used as the terrain digital elevation data. This data has been processed to fill data voids and may be ready to use in many common uses.

To standardize areas with mangroves in the PMM based on global mangrove conditions, we used the GMW 2020 data from Bunting *et al.* (2022) by clipping the PMM boundary. The resulting file was used to compute the abovementioned indices. Additionally, it was also used when applying an extract by mask to identify areas with mangroves from the EC spatial model and SRTM, to characterize them.

Spectral indices, the EC spatial model, and the SRTM digital elevation model were resampled at a 50-m pixel size. The latter was chosen because the study context involves preparing maps that will facilitate the installation of plots in the PMM for mangrove biomass monitoring, following Kauffmann and Donato (2012), who suggested a plot size of 50 m \times 50 m. By doing so, the pixel size will match the field plot size for further analysis.

Using the developed decision tree, we classified mangrove areas using GEE, an online platform for processing satellite data (Velastegui-Montoya *et al.*, 2023). The classification conditions are presented in Table 1 below. The decision tree approach threshold-based classification is justified in reducing the effect of correlation issues on input data (Breiman *et al.*, 1984; Cutler *et al.*, 2007; Hastie *et al.*, 2009; Kodikara et Woldai, 2017; Kavhu *et al.*, 2021). The area of each class was calculated as the product of the pixel counts and the pixel size in the final classification (50 m \times 50 m), as explained above. The classification layer was

projected at 4326 EPSG (European Petroleum Survey Group) System and World Geographic System 84 (WGS-84) datum.

We applied for a binary (mangroves, non-mangroves) validation of the classification map. We have computed a binary map using the reclassify tool available in ArcGIS 10.8 (Spatial Analyst Toolbox), after the final classification exportation from GEE to ArcGIS, to combine disturbed and undisturbed mangroves into a single class called 'mangroves'. Then, the result was a classification with only two classes: non-mangroves and mangroves. We performed a random stratified validation approach. Therefore, 430 points were randomly generated in our classification, split equally between mangrove (disturbed and

undisturbed) and non-mangrove classes. These points were overlaid onto a Planet-Nicfi 4.77 m spatial resolution image of January/February 2025, which was available in Collect Earth Online (Bey *et al.*, 2016) and classified again as mangrove and non-mangrove classes by a parallel validation classification process. Using a hands-on script in Google Earth Engine, a confusion matrix was produced from the results of the parallel validation on the binary reclassified image. We applied bias-corrected area estimation using the confusion matrix adjusted to area proportion pixel counts, as recommended by Olofsson *et al.* (2014) and implemented by Leite *et al.* (2018). The classification was assessed using overall, user, and producer accuracy.

Table 1. Decision Trees classification criteria

N°	Mangroves classes	NDVI	CMRI	NDMI	EC(μ S/ cm)	Elevation (meters)
1	Disturbed Mangrove	0.3 - 0.55	CMRI \geq 0.3	NDMI > 0.1	EC > 30 or EC < 0 (mask)	0-46
2	Non-disturbed Mangrove	0.55-1	CMRI > 0.5	NDMI > 0.1	EC > 30 or EC < 0 (mask)	0-46
3	Non-Mangrove	All other values				

Legend: NDVI: Normalized Difference Vegetation Index, CMRI: Combined Mangrove Recognition Index, NDMI: Normalized Difference Moisture Index, EC: Electrical Conductivity

3. RESULTS

3.1. Elevation, spectral vegetation index, and salinity variation in the PMM

The SRTM (Figure 2) data reported an altitude variation between 0 and 46 meters in the area with mangroves in the PMM. For the entire PMM, the highest elevation value reported was 163 meters, and the lowest was -14 meters. Figure 3 presents the variation of NDVI values. The highest value for the whole PMM was 0.87, while the minimum was -0.42. The minimum value for the areas with mangroves was -0.23, with the maximum of 0.82. The standard deviation for the whole PMM was 0.23, and the mean value was 0.48. The standard deviation of areas with mangroves was 0.11, and the mean value was 0.68.

Concerning the NDMI, the minimum value was -0.16 in areas with mangroves and -0.8 in the entire PMM. The maximum value was 0.71 across the whole PMM and 0.61 in areas with mangroves. The standard deviation was 0.20 in the PMM, with a mean value of 0.13. Conversely, in the regions with mangroves, the standard deviation value was 0.28, with a mean value of 0.29. Figure 4 presents the variation of NDMI.

Regarding the CMRI (Figure 5), the minimum value across the entire PMM was -0.79, and the maximum was 1.62, with a standard deviation of

0.42 and a mean of 0.94. In the mangrove zones, the minimum was -0.34, and the maximum was 1.55. The mean value was 1.18, with a standard deviation of 0.20. Visualizing the CMRI map reveals that CMRI does not clearly distinguish different vegetation types in the PMM. Low NDVI and CMRI values in mangrove areas indicate signs of disturbance or potential lack of mangrove classes in some areas expected to contain mangroves by GMW 2020.

Regarding electrical conductivity (EC) as a salinity proxy (Figure 6), values vary throughout the PMM, ranging from 0 μ S/cm to 34.705 μ S/cm (assuming that negative values were excluded as predictions). These values cover the freshwater to polyhaline water. For areas with mangroves, the mean EC value is 4078 μ S/cm.

According to the value range in Table 2 and Figure 6 below, the mangrove's location covers a small freshwater area. They are essentially in oligohaline and mesohaline waters and are sparse in polyhaline waters. In the white area, we have unpredictable values and artefact prediction with negative values. Some of the areas in white are located within the Global Mangroves Watch (GMW) area in the PMM but were unsampled during the field water EC measurement campaign due to accessibility

constraints, which may cause the negative predictions due to the lack of near-field data. They were masked because they don't have any physical meaning. It can be observed that these mangrove areas are located in the transition zone between oligohaline and freshwater environments. This will

be used in the classification process by applying a mask to the negative values to be included in the decision tree (Table 1). But other areas in white are clearly where we don't have mangroves, according to GMW. So, they will be mapped as non-mangrove pixels.

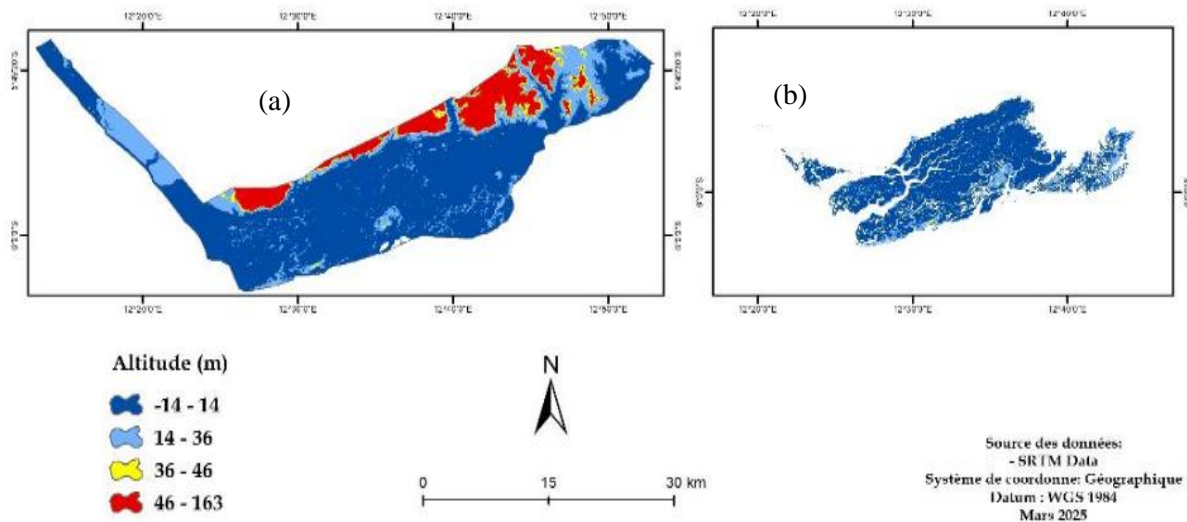


Figure 2. Variation of elevation from SRTM data in the whole PMM (a) and areas with mangroves (b)

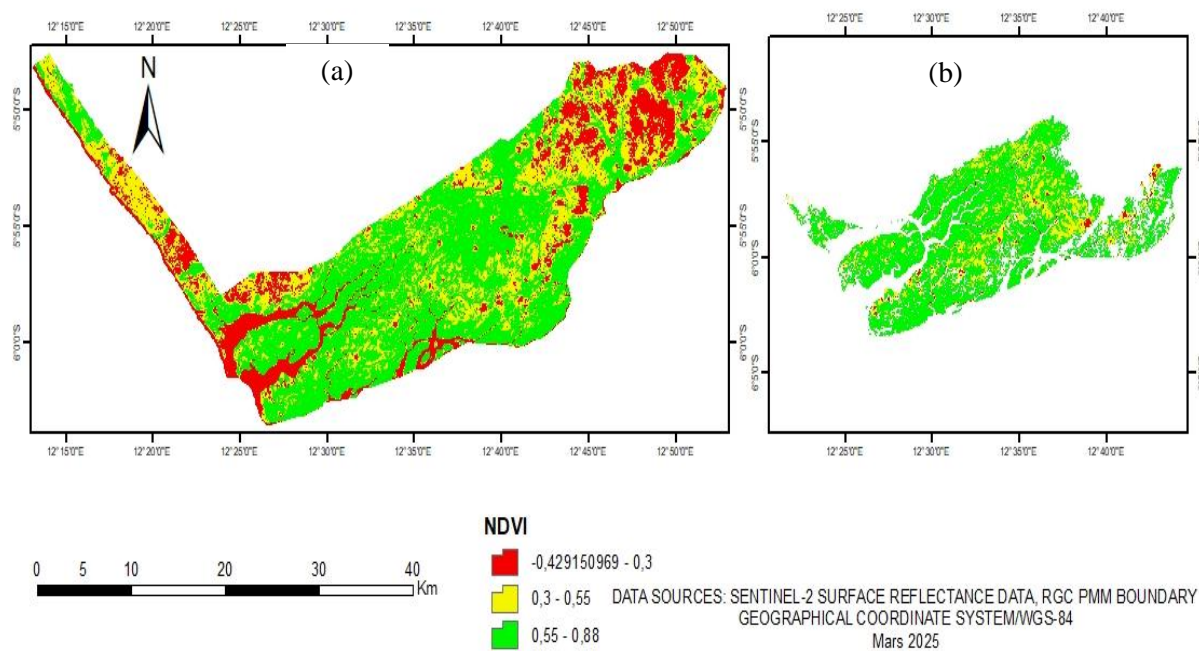


Figure 3. Variation of Normalized Difference Vegetation Index (NDVI) value in the whole PMM (a) and areas with mangroves (b)

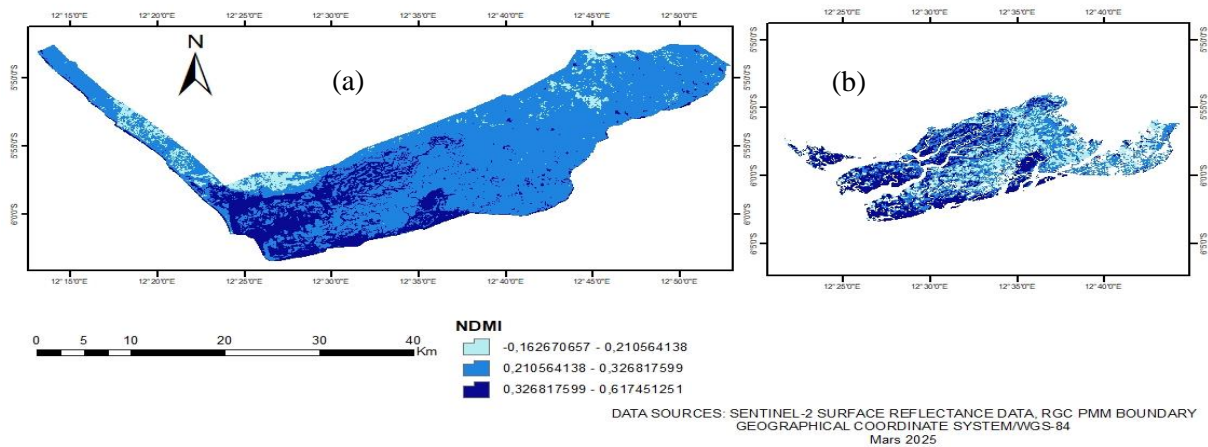


Figure 4. Variation of Normalized Difference Moisture Index (NDMI) in the whole PMM (a) and areas with mangroves (b)

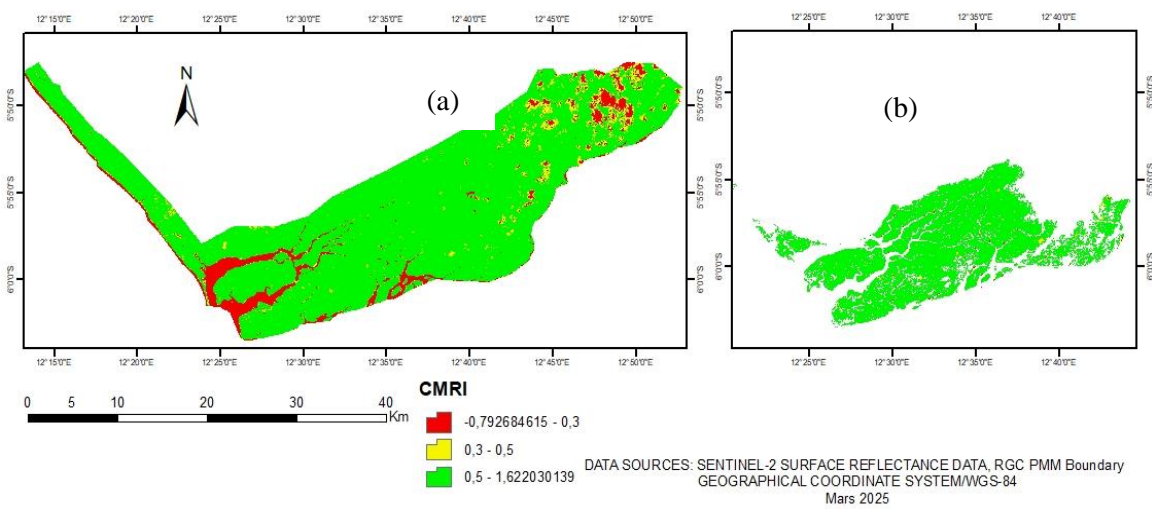


Figure 5. Variation of Combined Mangroves Recognition Index (CMRI) in the whole PMM (a) and areas with mangroves (b)

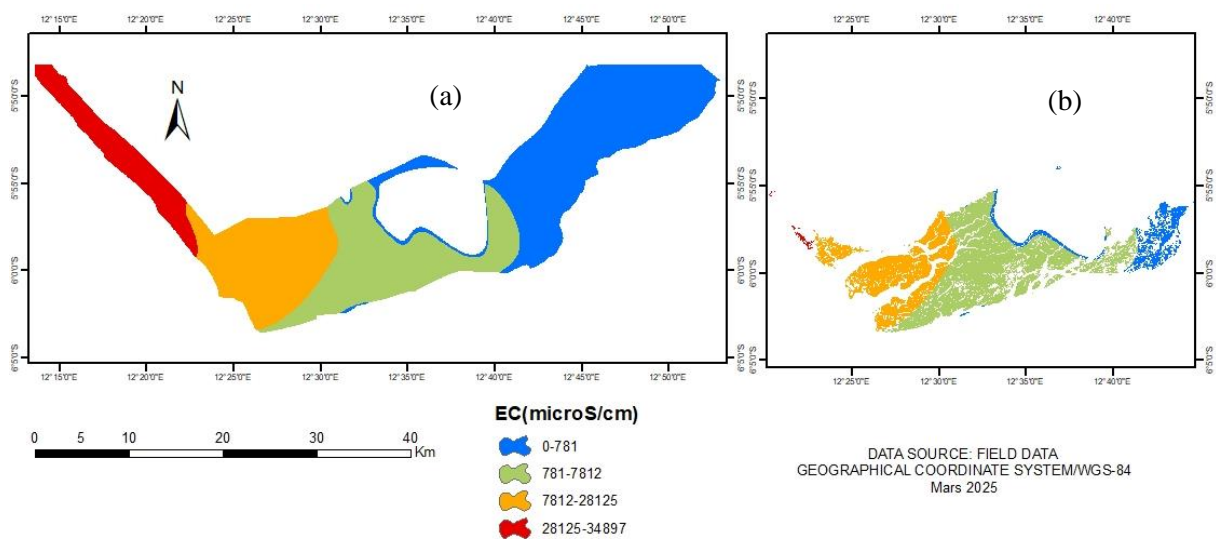


Figure 6. Variation of Electrical Conductivity, EC (as a proxy of salinity) in the whole PMM (a) and areas with mangroves (b)

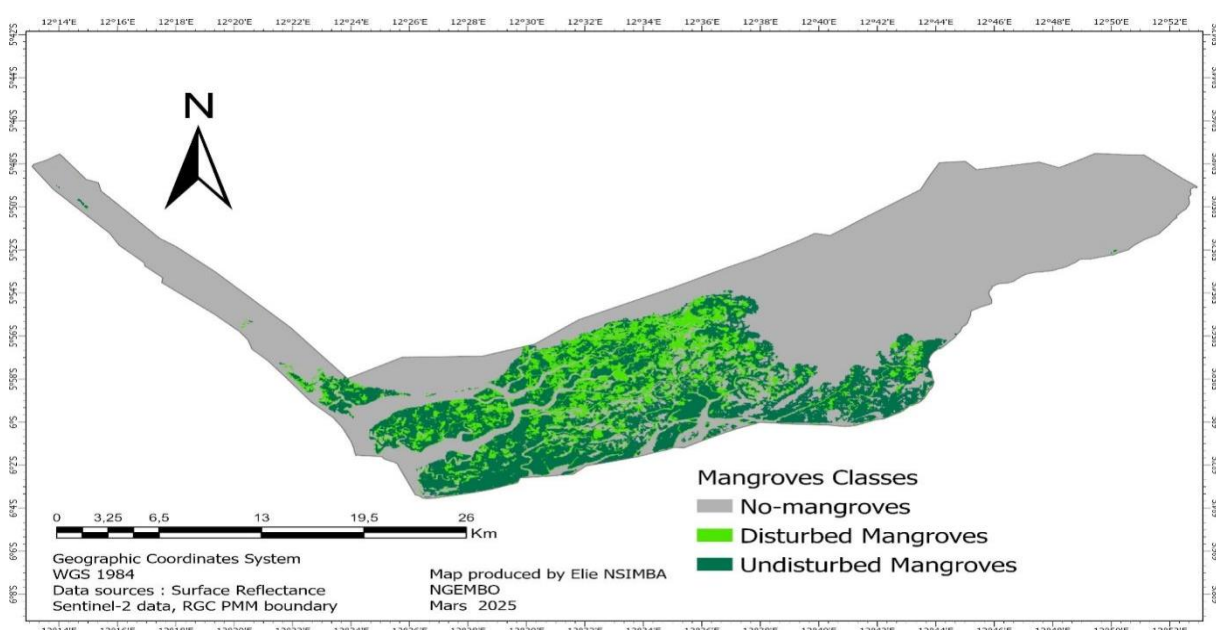
Table 2 below presents the electrical conductivity range and the salinity range classification according to the Venice classification in the PMM.

Table 2. Electrical conductivity (EC) value range in the PMM and salinity equivalence

N°	EC-value ($\mu\text{S}/\text{cm}$)	Equivalent Salinity value (ppt)	Equivalent salinity classification
1	0-781	0 - 0.5	Freshwater
2	781-7812	0.5-5	Oligohaline
3	7812 -28125	5-18	Mesohaline
4	28125-46975	18-30	Polyhaline

3.2. Mangrove degradation map, binary classification, and area estimations

Figure 7 presents the mangrove's location in two disturbance degrees in the PMM and the area of mangrove absence. These results indicate that mangroves are primarily located in the central region of the PMM, with degradation spatially distributed across many pixels. The non-mangrove class (NM) dominates the western and eastern parts of the PMM. Table 3 presents the area estimated for each mangrove degradation class using the pixel-based approach. It is shown that the NM zones represent an area of 487.24 km² (66.77%), while 76.89 km² is allocated to Disturbed Mangroves (DM) (10.53%), and 165.51 km² (22.68%) to Undisturbed Mangroves (UDM). This study estimates the total mangrove area (DM and UDM) to be 242.4 km².

**Figure 7.** Mangrove degradation state in the PMM**Table 3.** Area estimated for mangrove classes in the PMM

Mangroves classes	Area (km ²)	Percentage (%)
NM	487.24	66.77
DM	76.89	10.53
UDM	165.51	22.68

Legend : NM: Non-mangroves, DM: Disturbed Mangroves, UDM: Undisturbed Mangroves

Figure 8 below presents the variation of mangrove disturbance classes throughout the salinity classes. It is shown that the non-mangrove (NM) class dominates the freshwater (90.41 %), mesohaline (51.32 %), and polyhaline (97.50 %) classes. The Disturbed Mangroves (DM) have a high percentage in oligohaline environments (20.35 %), followed by 14.18 % in mesohaline environments. Freshwater and polyhaline have approximately 1.4 % of the DM.

The Undisturbed Mangroves (UDM) have a high proportion in the oligohaline areas (48.55 %), followed by mesohaline regions (34.49 %). In freshwater, they cover only 6.22 %, and in the polyhaline, they cover 1.07%. For the Unpredicted salinity areas (negative predictions that were masked), in the transition between oligohaline and freshwater, the UDM has a high proportion (46.22 %), followed by DM (36.70 %), and finally NM (17.07 %).

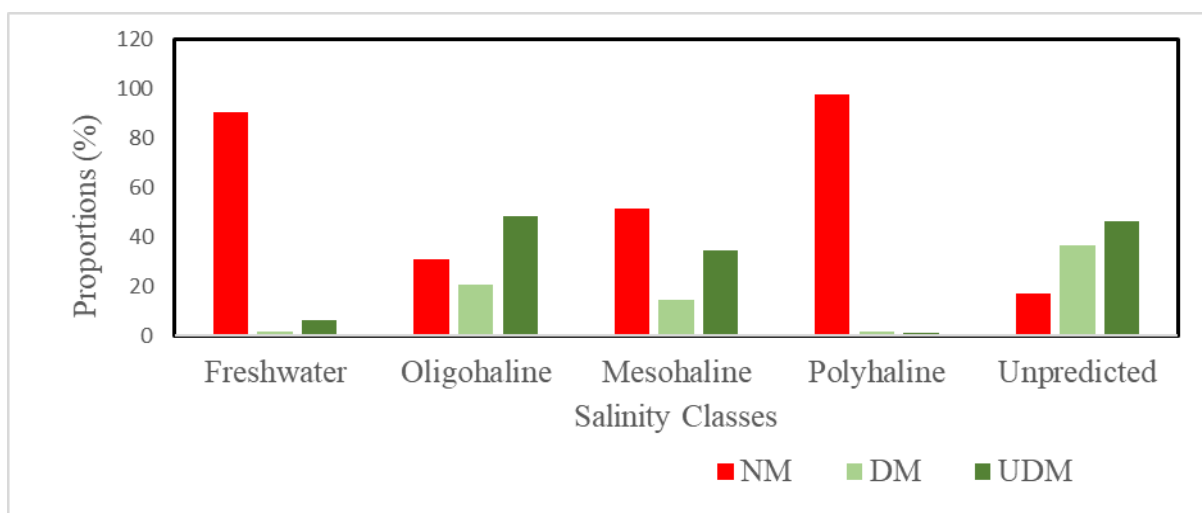


Figure 8. Variation of mangrove disturbance by salinity class predicted by interpolation (NM: no-mangroves, DM: Disturbed Mangroves, UDM: Undisturbed Mangroves).

Figure 9 below presents the location of mangrove disturbance states within the delineation of salinity range classification from the interpolation result.

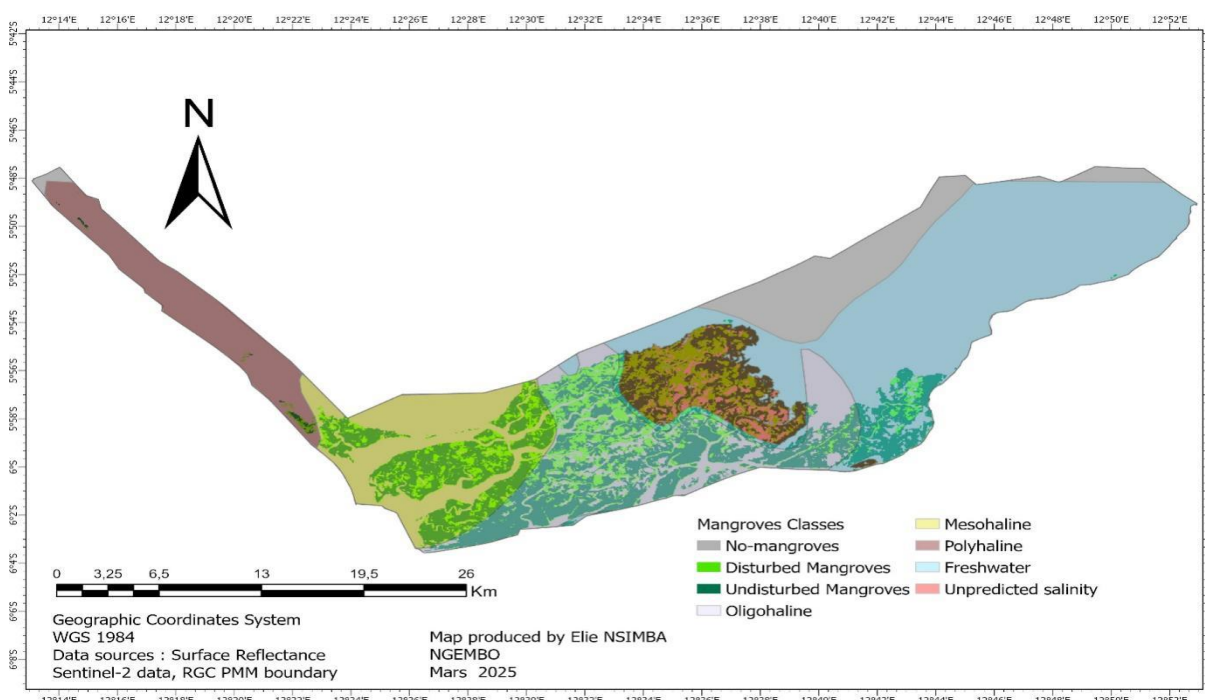


Figure 9. Mangrove disturbance classes overlaid by salinity prediction range

Table 4 presents the classification validation using a binary approach (mangroves and non-mangroves areas). The user and producer accuracies are reported to be higher than 95.00 %, with an overall accuracy of 96.90%. Areas with uncertainty estimation at the 95.00 % confidence level are $487.18 \pm 11.98 \text{ km}^2$ for non-mangrove areas, and $242.46 \pm 11.98 \text{ km}^2$ for mangrove areas. Figure 10 below shows the resulting binary map.

Table 4. Binary classification areas estimation with uncertainty (95 %)

Binary classes	User's Accuracy (%)	Producer's Accuracy (%)	Area with uncertainty estimation (95 %)	Overall Accuracy (%)
Non-mangroves	97.67	97.68	487.18 ± 11.98	96.90
Mangroves	95.34	95.32	242.46 ± 11.98	

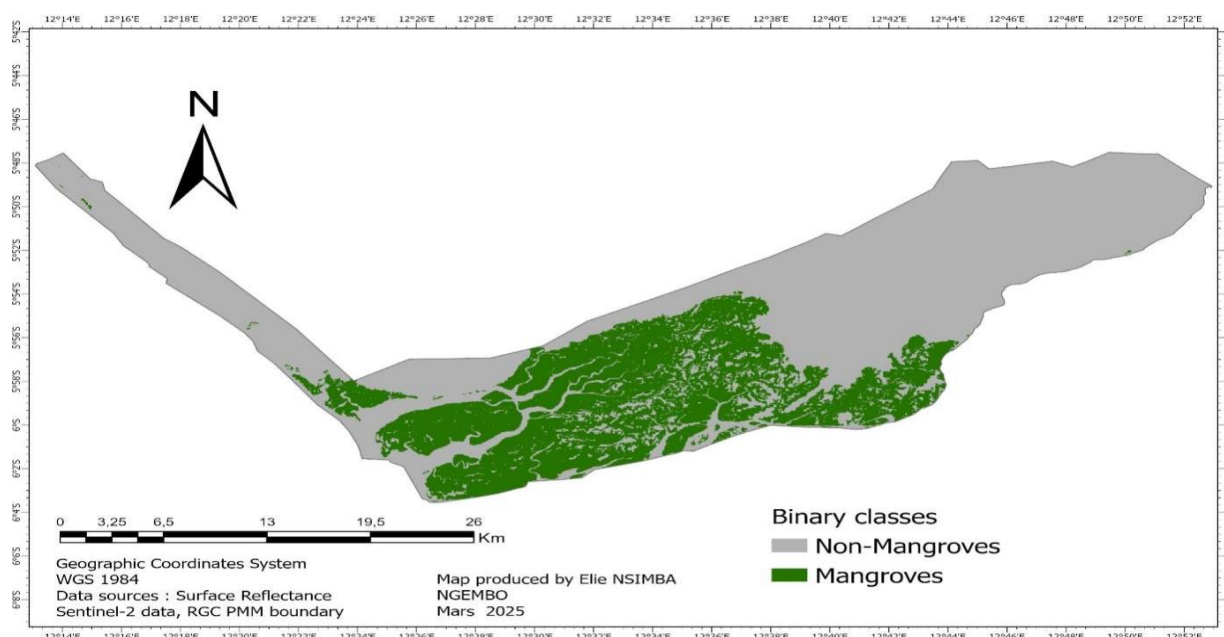


Figure 10. Binary classification of mangrove presence

4. DISCUSSION

4.1. SRTM data in mangrove mapping and characterization

SRTM data in the condition of mangrove ecosystems may explain more than terrain elevation. Due to interferences and perturbations in the interferometric system, SRTM elevation may explain tree heights instead of the exact terrain elevation. SRTM was designed to measure elevation, but due to the interaction of the short radar microwave with the canopy volume, the SRTM elevation measurement is biased by forest height and density (Simard, 2019). The canopy backscatter may have a higher influence on the radar shortwave used in SRTM than the ground to capture terrain variation precisely (Li *et al.*, 2022), which suggests that, with this assumption, forested hilltops appear higher than they are. Simard (2019) and Simard *et al.* (2006) explained the complex interactions between radar waves and mangrove canopies. He reported that, assuming mangroves are located at mean sea level (around null elevation) with negligible topography, the SRTM elevation measurement is directly related to mangrove canopy height. While this may be a gross assumption in mangrove regions with high tides (>3 m), it provides a robust method for determining patterns of mangrove height and biomass (Fatoyinbo *et al.*, 2013, 2018; Chen *et al.*, 2023).

This suggests that the SRTM value detected or used in this study in some areas may refer to mangrove heights rather than terrain elevation. So, the higher elevation value in mangrove areas may suggest taller mangrove trees in the PMM in some areas. Then, in the mangrove ecosystem, SRTM may provide critical information for biomass estimation,

servicing as a source of information on the height of mangrove trees.

4.2. NDVI (Normalized Difference Vegetation Index) values for mapping mangroves

This study uses a minimum value of 0.3 to map disturbed mangroves and a threshold value greater than 0.55 for undisturbed mangroves. The NDVI mean value for the mangrove zones, at 0.68, as shown in the NDVI description, indicates a value range typical of primary forest, which is considered non-disturbed mangrove. The standard deviation inside the mangrove areas is lower (0.11). This shows that mangroves are less disturbed globally in the PMM.

Despite this, the map reveals spatial variability in degraded NDVI values. Many pixels of low-value NDVI are sparse in the areas with mangroves, which may express the location of species mixtures or degradation. Studies support that mangroves can be mapped with a minimal NDVI value of 0.3, as reported by Yang *et al.* (2024). Taillie *et al.* (2024), studying the dieback of mangroves, reported that an NDVI value higher than 0.2 may be used to map disturbed mangroves. Kimera *et al.* (2024) mapped dense mangroves in Indonesia using the NDVI from 0.3. Akhtar *et al.* (2024) reported that dense mangroves have an NDVI value between 0.55 and 0.85. This matches the minimum threshold of 0.55 used in this study to classify mangroves as undisturbed. All these reports justify the NDVI minimum value of 0.3 used for disturbed mangroves, as well as the other thresholds employed in this study to map the state of mangrove disturbances.

4.3. Combined Mangroves Recognition Index (CMRI) values for areas with mangroves

Studies have reported that CMRI can improve the map accuracy of mangroves by more than 77% (Gupta *et al.*, 2018). Our analyses revealed that CMRI (Figure 5) does not highlight variation in vegetated areas in the PMM. Indeed, CMRI expresses forest cover within wetlands. In the context of PMM, where various vegetation physiognomies colonize wetlands, mainly due to human activities, CMRI may struggle to produce a precise result of differences within vegetation.

We used a threshold of 0.3 as the minimum value to map disturbed mangroves and 0.5 as the minimum value to map undisturbed mangroves. Sackey-Addo *et al.* (2020) found that the average minimum CMRI value required to map mangroves was approximately 0.46. Perea *et al.* (2021) and Huang *et al.* (2024) reported similar results. Compared to Valderrama-Landeros *et al.* (2024), our CMRI map didn't show a net separation between mangrove and non-mangrove areas or between mangrove disturbance states. This highlights the importance of utilizing multiple indices, rather than relying solely on CMRI, to map mangrove areas in the PMM.

4.4. NDMI (Normalized Difference Moisture Index) values for areas with mangroves

Although the minimum NDMI value for mangrove areas was reported as -0.16, our study used a minimum value of 0.1 to map mangroves. It is assumed that mangroves are more moisture-tolerant as they are subjected to more flooded conditions. This value falls within the range proposed by Ha *et al.* (2023), with a minimum value of -0.34 for NDMI in areas with mangroves.

4.5. Mangroves' presence and salinity

Mangroves were mapped to have a dense presence in areas within oligohaline and mesohaline waters (Figure 6, Table 2, Figures 8 and 9). This indicates the accommodation of mangrove species in moderate salinity levels, as reported by Samsuri *et al.* (2024) and Kimera *et al.* (2024), who found that mangroves thrive in salinity levels below 20 parts per thousand (20,000 ppm, 31,250 $\mu\text{S}/\text{cm}$). We have some mangroves in the transition between oligohaline and freshwater (unpredicted zones). Freshwater predicted near the oligohaline also shows the presence of mangroves. A very sparse and isolated distribution of mangrove zones has been revealed in the polyhaline water. The situation of mangroves in polyhaline water, high rates of non-mangroves, and disturbed mangroves may also be explained by the highest level of human activities and urbanization. Therefore, salinity was not the primary variable in detecting mangrove

degradation. According to our decision tree, undisturbed or disturbed mangroves were detected in the same salinity value range.

4.6. Main variables of mangrove disturbance detection.

It is worth noting that this study has analyzed pixels that were already classified as mangroves by Global Mangroves Watch. Following our decision tree, there are two main variables for detecting the disturbed state of mangroves: NDVI and CMRI. EC (as a proxy for salinity), NDMI, and elevation are within the same value range for both disturbed and undisturbed mangroves. They are secondary variables in this analysis. This reduces the effect of mask application or inaccurate salinity estimation for some areas on the characterization of mangrove stands.

4.7. Precautions in the interpretation of mangrove class areas and the need for an inventory of mangrove species distribution in the PMM

The classification produced and areas estimated in this study must be linked to the NDVI, CMRI, and NDMI fixed values of the decision trees mapping. Changes in the threshold of these values will impact the areas of each class. However, this is also linked to the Global Mangrove Watch feature, produced by Bunting *et al.* (2022), which serves as the standard global condition for mangrove areas. This feature lacks consideration of local species distribution or potential new colonization, which a field inventory would provide. The lack of a comprehensive mangrove inventory makes it challenging to produce an accurate map of mangrove presence, particularly when the local socio-ecological context must be taken into account.

The lack of confidence in predicting salinity values in some areas challenges the capture of the full mangrove's salinity pattern, even though these areas can be classified undoubtedly as being in the transition between oligohaline and freshwater. This situation suggests further research to characterize the electrical conductivity values in areas where this study was challenged, due to an issue with the spatial representation of field data, which is essentially explained by the difficulties in accessing some areas in the PMM during the field campaign.

5. CONCLUSION

This study mapped the state of mangrove degradation in the PMM using spectral indices, elevation data, and a spatial salinity model. Decision trees, based on a threshold in each degradation class, were used as a classification approach.

The results indicate spatial variability in mangrove degradation in the PMM, with wider areas of undisturbed mangroves (165.51 km², 22.68%) than disturbed mangroves (76.89 km², 10.53%). Mangroves are densely present in the oligohaline and mesohaline salinity classes. The lack of exhaustive mangrove species distribution in the PMM makes it challenging to produce an accurate map according to local ecological conditions. More information on environmental conditions, such as a complete salinity profile with other physicochemical properties in the PMM and species distribution, will be necessary for future mapping and a deeper understanding of mangrove functioning in the PMM.

A complete mangrove inventory in the PMM, even where Global Mangroves Watch has not mapped them, will improve our understanding of mangrove species distribution and degradation status, deepen our understanding of local mangrove ecological conditions, and increase our knowledge of the PMM flora, allowing us to produce a more accurate map of mangroves in the PMM.

Acknowledgements

We thank the ISOFYS Laboratory of Ghent University, Faculty of Biosciences, for providing us with the Hanna Instrument for the water EC measurement field mission. We also thank the European Union through ERAIFT and AGRINATURE-GEIE for the financial support, which was essential for our journey in the Parc Marin des Mangroves. We are grateful to all the Staff of the Institut Congolais pour la Conservation de la Nature (ICCN, in short), including those in the central office in Kinshasa and the Moanda team in the Parc Marin des Mangroves.

References

- Akhtar N. & Tsuyuzakin S., 2024. Effects of disturbances on the spatiotemporal patterns and dynamics of coastal wetland vegetation. *Ecological Indicators*, 166, 112430, 12. <https://doi.org/10.1016/j.ecolind.2024.112430>
- Allais L., Thibodeau B., Khan S.N., Crowe A.S., Cannicci S. & Not C., 2024. Salinity, mineralogy, porosity, and hydrodynamics as drivers of carbon burial in urban mangroves from a megacity. *Science of The Total Environment*, V912, 168955, 17. <https://doi.org/10.1016/j.scitotenv.2023.168955>
- APHA, AWWA & WEF, 2017. *Standard Methods for the Examination of Water and Wastewater* (23rd ed.). American Public Health Association, American Water Works Association, Water Environment Federation, 2671 p. ISBN: 978-0-87553-287-5
- Baloloy A. B., Blanco A. C., Blanco R. R., Ana C. S. & Kazuo N., 2020. Development and application of a new mangrove vegetation index (MVI) for rapid and accurate mangrove mapping. *ISPRS Journal of Photogrammetry and Remote Sensing*, 166, 95–117. <https://doi.org/10.1016/j.isprsjprs.2020.06.001>
- Bey A., Sánchez-Paus Díaz A., Maniatis D., Marchi G., Mollicone D., Ricci S., Bastin J.-F., Moore R., Federici S., Rezende M. *et al.*, 2016. Collect Earth: Land Use and Land Cover Assessment through Augmented Visual Interpretation. *Remote Sens*, 8, 807, 24. <https://doi.org/10.3390/rs8100807>
- Bhowmik A. K., Padmanaban R., Cabral P. & Romeiras M.M., 2022. Global Mangrove Deforestation and Its Interacting Social-Ecological Drivers: A Systematic Review and Synthesis. *Sustainability*, 14(8), 4433. <https://doi.org/10.3390/su14084433>
- Bunting P., Rosenquist A., Hilarides L., Lucas R.M., Thomas N., Tadono T., Worthington T.A., Spalding M., Murray N.J., & Rebelo L.-M., Global Mangrove Extent Change 1996–2020: Global Mangrove Watch Version 3.0. *Remote Sens*, 2022,14, 3657, 32. <https://doi.org/10.3390/rs14153657>
- Breiman L., Friedman J., Stone C. J. & Olshen R.A., 1984. *Classification and Regression Trees*. 368 p. <https://doi.org/10.1201/9781315139470>
- Chen R., Rong Z., Chuanpeng Z., Zongming W. & Mingming J., 2023. High-Resolution Mapping of Mangrove Species Height in Fujian Zhangjiangkou National Mangrove Nature Reserve Combined GF-2, GF-3, and UAV-LiDAR. *Remote Sensing* 15(24), 5645, 17. <https://doi.org/10.3390/rs15245645>
- Cutler D.R., Edwards T.C. Jr., Beard K.H., Cutler A., Hess K.T., Gibson J. & Lawler J.J., 2007. Random Forests For Classification In Ecology. *Ecology*, 88, 2783-2792. <https://doi.org/10.1890/07-0539.1>
- Fatoyinbo T.E. & Simard M., 2013. Height and biomass of mangroves in Africa from ICESat/GLAS and SRTM. *International Journal of Remote Sensing*, 34(2), 668-681. <https://doi.org/10.1080/01431161.2012.712224>
- Fatoyinbo T., Feliciano A.E., Lagomasino D., Lee S.K. & Trettin C., 2018. Estimating mangrove aboveground biomass from airborne LiDAR data: A case study from the Zambezi River delta. *Environmental Research Letters*, 13(2), 025012, 13. <https://doi.org/10.1088/1748-9326/aa9f03>
- Faye M. N., Guissé A. & Diallo N., 2007. Influence du pH, de la salinité de l'eau et de la texture du sol sur la végétation de la mangrove de l'estuaire du Saloum au Sénégal. *Journal des Sciences Environnementales*, 35(3), 200–215. http://jst.ucad.sn/images/stories/articles/volume5_1/vol5_1_2.pdf
- Gorelick N., Hancher M., Dixon M., Ilyushchenko S., Thau D. & Moore R., 2017. Google Earth Engine: Planetary-scale geospatial analysis for everyone. *Remote Sens. Environ.*, 202, 18–27. <https://doi.org/10.1016/j.rse.2017.06.031>
- Greenfield E., 2024. Les mangroves des Maldives se noient dans l'eau salée à mesure que le niveau de la mer monte. *Journal of Coastal Ecology*, 42(2), 123–138. <https://sigmaearth.com/fr/Les-mangroves-des-Maldives-se-noient-dans-l%27eau-sal%3%A9e-%C3%A0->

[mesure-que-le-niveau-de-la-mer-monte/](#) consulté le 08 avril 2025.

Gupta K., Mukhopadhyay A., Giri S., Chanda A., Majumdar D.S., Samanta S., Mitra D., Samal N. R., Pattnaik K.A. & Hazra S., 2018. An index for discrimination of mangroves from non-mangroves using LANDSAT 8 OLI imagery. *Methods X*, 5, 1129-1139. <https://doi.org/10.1016/j.mex.2018.09.011>

Ha T.S., Nguyen H.H. & Truong V.V., 2023. Mangrove cover-based vegetation indices mapping using PlanetScope data in Tien Yen District, Quang Ninh Province. *Journal of Forestry Science and Technology*, 15, 127-138. <https://doi.org/10.55250/jo.vnuf.2023.15.127-138>

Hastie T., Tibshirani R. & Friedman J., 2009. *The Elements of Statistical Learning: Data Mining, Inference, and Prediction*. (2nd ed.), pp. 214-233. <https://link.springer.com/book/10.1007/978-0-387-84858-7>

Huang K., Yang G., Sun W., Fu B., Chen C., Meng X., Feng T. & Wang L., 2024. The phenology and water level time-series mangrove index for improved mangrove monitoring. *International Journal of Applied Earth Observation and Geoinformation*, 134(104188), 1569-8432. <https://doi.org/10.1016/j.jag.2024.104188>

Kauffman J.B. & Donato D.C., 2012. Protocols for the Measurement, Monitoring and Reporting of Structure, Biomass and Carbon Stocks in Mangrove Forests. *Working Paper 86, CIFOR, Bogor*. 50 p. https://www.cifor-icraf.org/publications/pdf_files/WPapers/WP86CIFOR.pdf

Kavhu B., Mashimbye Z. E., & Luvuno L., 2021. Climate-Based Regionalization and Inclusion of Spectral Indices for Enhancing Transboundary Land-Use/Cover Classification Using Deep Learning and Machine Learning. *Remote Sensing*, 13(24), 5054, 23. <https://doi.org/10.3390/rs13245054>

Kimera F., Sobhi B., Omara M. & Sewilam H., 2024. Impact of Salinity Gradients on Seed Germination, Establishment, and Growth of Two Dominant Mangrove Species Along the Red Sea Coastline. *Plants*, 13(24), 3471, 15. <https://doi.org/10.3390/plants13243471>

Kodikara G. R. L. & Woldai T., 2017. Spectral indices derived, non-parametric Decision Tree Classification approach to lithological mapping in the Lake Magadi, Kenya. *International Journal of Digital Earth*, 11(10), 1020-1038. <https://doi.org/10.1080/17538947.2017.1372525>

Leite A., Cáceres A., Mills M., Melo M. & Monteiro A.T., 2018. Reducing Emissions from Deforestation and Forest Degradation in Angola: insights from the Scarp Forest conservation 'hotspot'. *Land Degradation and Development*, 29(12), 4291-4300. <https://doi.org/10.1002/ldr.3178>

Li Y., Haiqiang F., Jianjun Z., Kefu W., Panfeng Y., Li W. & Gao S., 2022. A Method for SRTM DEM Elevation Error Correction in Forested Areas Using ICESat-2 Data and Vegetation Classification Data. *Remote Sensing* 14(14), 3380, 12. <https://doi.org/10.3390/rs14143380>

Mbiya K. J., Opey A.J. & Makanzu I.F., 2024. Study of the spatio-temporal dynamics of the Mangrove Marine Park (PMM) on the Atlantic coast of Muanda, DR Congo. *Afrique Science*, 24(4), 59-68. <https://www.africainscience.net/admin/postpdfs/d7741e192859d5f7b55a2a035b6cd3021715767375.pdf>

Martínez F.B.I., Rueda M., Ferrin O.O.O., Díaz-Ochoa J.A., Castillo-Vargasmachucas S. & Selvaraj J.J. 2024. A novel approach for improving the spatiotemporal distribution modeling of marine benthic species by coupling a new GIS procedure with machine learning. *Deep Sea Research Part I. Oceanographic Research Papers*, 203, 104222, 17. <https://doi.org/10.1016/j.dsr.2023.104222>

Martínez-Fonseca J.G., Westeen E.P., Jenness J., Zahratka J.L. & Chambers C.L., 2024. Species distribution models predict potential habitat for the endangered New Mexico jumping mouse. *The Journal of Wildlife Management*, 88(8), e22646. <https://doi.org/10.1002/jwmg.22646>

Merow C., Galante P. J., Kass J. M., Aiello-Lammens M.E., Babich Morow C., Gerstner B. E., Grisaales Betancur V., Moore A.C., Noguera-Urbano E. A., Pinilla-Buitrago G. E., Velásquez-Tibatá J.e., Anderson R. P. & Blair M.E. 2022. Operationalizing expert knowledge in species' range estimates using diverse data types. *Merow et al. Operationalizing expert knowledge in SDMs. Frontiers of Biogeography*, 14(2), e53589.18p. <https://doi.org/10.21425/F5FBG53589>

Muyaya K.B., Rudant J.P., Lumbuenamo S.R., Muamba M.P., Wayawo M P., Konunga M.G. & Collet M., 2017. Assessment of the potential of satellite imagery Sentinel-1 and Sentinel-2 for mapping the mangrove marine park in the Democratic Republic of Congo. *International Journal of Innovation and Applied Studies*, 21(3), 398-409. <https://ijias.issr-journals.org/abstract.php?article=IJIAS-17-066-01>

Olofsson P., Foody G. M., Herold M., Stehman S. V., Woodcock C. E. & Wulder M. A., 2014. Good practices for estimating area and assessing the accuracy of land change. *Remote Sensing of Environment*, 148, 42-57. <https://doi.org/10.1016/j.rse.2014.02>

Perea M., Villamil L.J. & Barrero O.F., 2021. Caracterización espectral y monitoreo de bosques de manglar con Teledetección en el litoral Pacífico colombiano: Bajo Baudó, Chocó. *La Granja*, 34(2), 18. <https://doi.org/10.17163/lgr.n34.2021.02>

Risanti A.A. & Marfai M. A., 2020. The effects of hydrodynamic process and mangrove ecosystem on sedimentation rate in Kendal coastal area, Indonesia. *IOP Conf. Ser.: Earth Environ. Sci.*, 451, 012070, 16. <https://doi.org/10.1088/1755-1315/451/1/012070>

Rouse J.W., Haas R.H., Schell J.A. & Deering D.W., 1973. Monitoring Vegetation Systems in the Great Plains with ERTS (Earth Resources Technology Satellite). *Proceedings of 3rd Earth Resources Technology Satellite Symposium, Greenbelt, 10-14 December, SP-351*, pp 309-317.

Sackey-Addo S., 2020. *Evaluating the performance of CMRI for estimating the spatial distribution of mangroves at the Keta Lagoon Complex in the Volta*

- Region of Ghana*. Thesis, University of Ghana, 72 p. <https://ugspace.ug.edu.gh/handle/123456789/42460>
- Samsuri M.R. A., Zaitunah A.A., Utomo B. & Sulistoadi J.B., 2024. Distribution of density and zoning patterns of mangrove forest in eastern coastal Sumatera, Indonesia. *IOP, Earth and Environmental Science*, 1352, 1-11. doi:10.1088/1755-1315/1352/1/012045
- Simard M., 2019. Radar Remote Sensing of Mangrove Forests. SAR Handbook: Comprehensive Methodologies for Forest Monitoring and Biomass Estimation. In *Eds. Flores, A., Herndon, K., Thapa, R., Cherrington, E., NASA*. <https://doi.org/10.25966/33zm-x271>
- Simard M., Zhang K., Ross M.S., Rivera-Monroy V.H., Castaneda-Moya E. & Twilley R., 2006. Using Shuttle Radar Topography Mission Elevation Data to Map Mangrove Forest Height in the Caribbean," 2006 *IEEE International Symposium on Geoscience and Remote Sensing, Denver, CO, USA*, pp. 1713-1716. <https://doi.org/10.1109/IGARSS.2006.443>
- Sunkur R., Kantamaneni K., Bokhoree C. *et al.*, 2024. Mangrove mapping and monitoring using remote sensing techniques towards climate change resilience. *Sci. Rep.*, 14, 6949, 14. <https://doi.org/10.1038/s41598-024-57563-4>
- Taillie P.J., Roman-Cuesta R., Lagomasino D., Cifuentes-Jara M., Fatoyinbo T., Ott L.E. & Poulter B., 2024. Widespread mangrove damage resulting from the 2017 Atlantic mega hurricane season. *Environ. Res. Lett.*, 15, 1-10. [10.1088/1748-9326/ab82cf](https://doi.org/10.1088/1748-9326/ab82cf)
- Tran T. V., Reef R. & Zhu X., 2022. A Review of Spectral Indices for Mangrove Remote Sensing. *Remote Sensing*, 14(19), 4868, 29. <https://doi.org/10.3390/rs14194868>
- Tran T.V., Reef R. & Zhu X., 2024. Long-term changes of mangrove distribution and its response to anthropogenic impacts in the Vietnamese Southern Coastal Region. *Journal of Environmental Management*, 370, 122658, 17. <https://doi.org/10.1016/j.jenvman.2024.122658>
- UNESCO (United Nations Educational, Scientific and Cultural Organization) 1958. The Venice System for the Classification of Marine Waters According to Salinity. In Anonym. Symposium on the Classification of Brackish Waters. *Archo Oceanogr. Limnol.*, 11 (Suppl.), 243-248.
- Valderrama-Landeros L., Troche-Souza C., Alcántara-Maya J.A., Velázquez-Salazar S., Vázquez-Balderas B., Villeda-Chávez E., Cruz-López M.I., Ressler R., Flores-Verdugo F. & Flores-de-Santiago F., 2024. An assessment of mangrove forest in northwestern Mexico using the Google Earth Engine cloud computing platform. *PLoS One*, 5,19(12), e0315181, 16. <https://doi.org/10.1371/journal.pone.0315181>
- Velastegui-Montoya A., Montalván-Burbano N., Carrión-Mero P., Rivera-Torres H., Sadeck L. & Adami M., 2023. Google Earth Engine: A Global Analysis and Future Trends. *Remote Sensing*, 15(14), 3675, 30. <https://doi.org/10.3390/rs15143675>
- Yang X., Zhu Z., Kroeger D.K., Qiu S., Covington S., Conrad R.J. & Zhu Z., 2024. Tracking mangrove condition changes using dense Landsat time series. *Remote Sensing of Environment*, 315, 114461, 20. <https://doi.org/10.1016/j.rse.2024.114461>
- Zhang H., Lu L., Liu Y. & Liu W., 2015. Spatial Sampling Strategies for the Effect of Interpolation Accuracy. *ISPRS International Journal of Geo-Information*, 4(4), 2742-2768. <https://doi.org/10.3390/ijgi4042742>